



Cite this: *RSC Adv.*, 2018, 8, 28002

## Adsorption characteristics of Cd(II) in aqueous solutions using spent mushroom substrate biochars produced at different pyrolysis temperatures†

Yang Xian, Jun Wu, \* Gang Yang, Ruiting Liao, Xiaohong Zhang, Hong Peng, Xiaoyu Yu, Fei Shen,  Li Li and Lilin Wang

To effectively remove Cd from water, biochars were produced by pyrolyzing surplus agricultural wastes of spent mushroom substrate (SMS) at 300, 500, and 700 °C. The biochars were characterized, and their Cd(II) removal ratios and adsorption capacities in aqueous solutions were evaluated. The physical and chemical properties of the biochars were significantly affected by increasing the pyrolysis temperature; the data indicated that the ash content, pH and specific surface area of the biochars increased, whereas the yield and contents of carbon, hydrogen, nitrogen and oxygen decreased. In addition, the molar ratios of H/C, O/C and (O + N)/C decreased, which implied that the biochars became more aromatic and carbonaceous with a lower polarity and fewer oxygen-based functional groups. The pseudo-second-order kinetics model and Langmuir and Temkin isotherm models described the Cd(II) adsorption better than the other tested models. The biochars derived at higher pyrolysis temperatures had higher adsorption capacities, and the maximum adsorption capacities for PC700 and SC700 were 71.49 and 46.87 mg g<sup>-1</sup>, respectively. The  $Q_m$  values in our study were equivalent to or even higher than those for other modified biochars. This result shows that the biochars in this study are effective adsorbents for Cd(II) removal from wastewater.

Received 9th May 2018  
Accepted 28th July 2018

DOI: 10.1039/c8ra03958e

rsc.li/rsc-advances

## Introduction

Spent mushroom substrate (SMS) is agricultural waste left over from mushroom cultivation and is generally composed of wheat straw, poultry manure and other ingredients.<sup>1</sup> China has become the world's largest producer of mushrooms, accounting for approximately 75% of the annual global mushroom production.<sup>2</sup> Each kilogram of mushrooms can produce approximately 5 kg of waste.<sup>3</sup> Consequently, tremendous amounts of SMS are generated from mushroom production, which has created a substantial challenge for waste disposal. Traditionally, SMS is used in fields as a fertilizer or incinerated; the latter method leads to severe environmental pollution.<sup>4</sup> In recent studies, SMS biochars have been used for fluoride removal from aqueous solutions<sup>5</sup> and for ammonium nitrogen adsorption.<sup>6</sup> However, limited research exists on the feasibility of using SMS derivatives to remove cadmium from aqueous solutions.

Heavy metal pollution in water has become one of the most severe environmental problems.<sup>7,8</sup> Heavy metals are ubiquitous, nonbiodegradable, and highly toxic to all living organisms,

including plants, animals, and humans.<sup>9–11</sup> Cadmium (Cd) is a nonessential heavy metal, and numerous anthropogenic activities directly or indirectly contribute to the enrichment of Cd in the environment. Cd contamination causes long-term and short-term effects in humans, and the major mechanism by which Cd is introduced into human bodies and other living organisms is through the food chain.<sup>8,12,13</sup> Therefore, the effective removal of Cd from water is of great importance.

Biochar is the solid by-product of biomass, such as wood, crop straw, sewage sludge and animal manure, that was subjected to pyrolysis under oxygen-limited conditions.<sup>14–16</sup> In recent years, biochar has drawn increasing attention due to its special physicochemical characteristics, including a large specific surface area, an abundance of pores and surface functional groups, and a high surface negative charge and charge density.<sup>17</sup> These properties allow the use of biochar as an adsorbent for organic and inorganic pollutants.<sup>18,19</sup> An increasing number of studies have shown that biochar can effectively remove heavy metals from aquatic environments,<sup>20,21</sup> and the type of biochar feedstock affects its intrinsic properties. To enhance the removal ratio and adsorption capacity of biochar for heavy metals, increasing numbers of studies have used a variety of methods to modify biochar. For example, W.-Q. Zuo *et al.* used CaCO<sub>3</sub> nanoparticles to modify sewage sludge biochar (CMSSB) to enhance the removal of Cd(II) from aqueous solution, and the adsorption capacity of the obtained CMSSB

College of Environmental Science, Sichuan Agricultural University, Chengdu 611130, P. R. China. E-mail: wuj1962@163.com

† Electronic supplementary information (ESI) available. See DOI: 10.1039/c8ra03958e



for Cd(II) based on the Langmuir model was  $36.5 \text{ mg g}^{-1}$ .<sup>22</sup> Y.-Y. Wang *et al.* used a  $\text{MnFe}_2\text{O}_4$ -biochar nanocomposite to simultaneously remove Sb(III) and Cd(II) from water; the results showed that the maximum adsorption capacities for Sb(III) and Cd(II) were 237.53 and  $181.49 \text{ mg g}^{-1}$ , respectively, in a bisolute system.<sup>23</sup> However, modifying biochar may cause secondary pollution, and modified biochar has a higher economic cost than common biochar. Ultimately, we can choose a biochar with a high adsorption capacity for heavy metals. In this study, the research on biochar preparation from SMS for wastewater treatment and the effects of different factors, such as the Cd concentration, contact time, initial pH, temperature and adsorbent doses, on the adsorption of Cd in aqueous solutions will provide theoretical references and technical support for the removal of Cd from water.

## Materials and methods

### Materials and reagents

SMSs were collected from the mushroom industry in Chengdu, China. The spent *Pleurotus ostreatus* substrate mainly consisted of bran (60%), corn cob (20%) and rice straw (20%). The spent shiitake substrate mainly consisted of sawdust (80%) and bran (20%). The collected SMSs were dried at  $105^\circ\text{C}$  for 12 h to remove any moisture and then milled into particles. The resulting particles (filtered through a 40-mesh sieve) were stored for subsequent use. The spent *Pleurotus ostreatus* substrate consisted of cellulose, hemicellulose and lignin with contents of 25.78%, 7.55% and 32.9%, respectively, and the spent shiitake substrate consisted of cellulose, hemicellulose and lignin with contents of 24.99%, 4.81% and 23.16%, respectively. Biochars were prepared by thermal treatment in an oxygen-limited atmosphere.<sup>5</sup> The prepared SMSs were weighed in crucibles with lids. The samples were carbonized at 300, 500 or  $700^\circ\text{C}$  in an airtight muffle furnace for 2 h and then cooled to room temperature. The different SMS biochars are referred to as PC300, PC500, PC700, SC300, SC500 and SC700 according to the preparation temperature and raw material type.

Analytical-grade cadmium nitrate tetrahydrate ( $\text{Cd}(\text{NO}_3)_2 \cdot 4\text{H}_2\text{O}$ ), NaOH, and HCl were procured from Sinopharm Chemical Reagent Co., Ltd. (Shanghai, China) and dissolved in deionized (DI) water ( $18.2 \text{ M}\Omega$ ) (Nanopure water, Barnstead, IO, USA).

### Characterization of the biochars

The biochar samples were analyzed using an elemental analyzer (MicroCube, Elementar, Germany) to determine the total C, H, N, O and S contents of the biochars. The pH values were measured in the supernatant of the biochar aqueous solutions (solid : water ratio of 1 : 20). The pore size distributions and surface areas were determined using the Brunauer–Emmett–Teller (BET) method with an ASAP 2020 surface area pore analyzer. The functional groups in the samples were identified using a TENSOR27 Fourier transform infrared (FT-IR) spectrometer (Bruker, Ettlingen, Germany). The oxygen-containing functional groups of the biochars were analyzed using the Boehm titration method.<sup>24</sup> The biochars ( $0.5 \text{ g}$ ) were mixed with

$50 \text{ mL}$  of  $0.05 \text{ M}$   $\text{NaHCO}_3$ ,  $\text{Na}_2\text{CO}_3$ , NaOH, or HCl in  $50 \text{ mL}$  tubes for 24 h. Then,  $0.1 \text{ M}$  HCl or NaOH was used to neutralize the excess base or acid, respectively, using a back-titration method. The oxygen-containing functional groups were determined based on the assumption that  $\text{NaHCO}_3$  neutralized the carboxyl groups,  $\text{Na}_2\text{CO}_3$  neutralized the carboxyl groups and lactones, NaOH neutralized all organic acids and acidic functional groups, including phenols, and HCl neutralized all alkaline groups.<sup>25</sup> The structures and morphologies of the biochars were observed by scanning electron microscopy (SEM). X-ray diffraction (XRD) analysis was conducted on a computer-controlled X-ray diffractometer (D/max 2500, Rigaku, Japan) equipped with a stepping motor and graphite crystal monochromator.

### Adsorption kinetics and isotherms

Stock solutions of Cd ( $1000 \text{ mg L}^{-1}$ ) were prepared by dissolving  $1.3721 \text{ g}$  of  $\text{Cd}(\text{NO}_3)_2 \cdot 4\text{H}_2\text{O}$  in deionized water ( $1000 \text{ mL}$ ). The adsorption kinetics of Cd(II) on the biochars was determined by adding  $0.2 \text{ g}$  of the biochars to  $100 \text{ mL}$  polyethylene (PE) centrifuge tubes containing  $50 \text{ mL}$  of the sorbate solution ( $100 \text{ mg L}^{-1}$  Cd(II)). The centrifuge tubes were maintained with constant shaking (at  $160 \text{ rpm}$ ) at room temperature ( $25 \pm 0.5^\circ\text{C}$ ) in a vapor-bathing constant temperature vibrator. Samples were taken at different time intervals (0, 0.5, 1, 2, 4, 8, 12 and  $24 \text{ h}$ ), and the solutions were separated by filtration. The Cd concentrations in the filtrates were determined using flame atomic absorption spectrometry (AAS, Thermo Solaar M6, Thermo Fisher Scientific Ltd., USA).

The adsorption isotherms of Cd(II) on the biochars were investigated by adding  $0.2 \text{ g}$  of the biochars to  $100 \text{ mL}$  PE centrifuge tubes containing  $50 \text{ mL}$  of the sorbate solution. The Cd concentration ranged from 20 to  $300 \text{ mg L}^{-1}$ . The centrifuge tubes were shaken in a mechanical shaker for 12 h at room temperature ( $25 \pm 0.5^\circ\text{C}$ ), and then, the samples were filtered to determine the Cd concentrations in the filtrates using the same method. The amount of Cd sorbed on the biochars ( $Q_e$ ) and the Cd removal efficiency ( $E$ ) were calculated according to the following equations:

$$Q_e = (C_o - C_e) \times V/m \quad (1)$$

$$E (\%) = (C_o - C_e)/C_o \times 100 \quad (2)$$

where  $C_o$  and  $C_e$  ( $\text{mg L}^{-1}$ ) are the initial and final (after adsorption) Cd concentrations, respectively,  $m$  ( $\text{g}$ ) is the dry weight of the biochar, and  $V$  ( $\text{mL}$ ) is the volume of the Cd solution.

### Effects of the dose and initial pH

Different amounts of biochar ( $1, 2, 4, 10, 20$ , and  $40 \text{ g L}^{-1}$ ) were added to  $100 \text{ mL}$  PE centrifuge tubes containing  $50 \text{ mL}$  of the sorbate solution ( $100 \text{ mg L}^{-1}$  Cd(II)) to study the effects of the biochar dose on Cd(II) adsorption. The effect of the initial pH was investigated by varying the solution pH (3–8) at a biochar dose of  $4 \text{ g L}^{-1}$ . After 12 h of shaking in a vapor-bathing



constant temperature vibrator at room temperature ( $25 \pm 0.5$  °C), the same methods were used to determine the Cd concentrations in the filtrates.

### Biochar reuse

To test the reusability of the SMS biochars, three consecutive cycles were performed in triplicate. Each adsorption process was carried out as a batch experiment for 12 h, and then the biochar was separated using centrifugation. Prior to the next cycle, the collected adsorbent was washed repeatedly to remove any residual solution.

### Statistical analyses

Each treatment was conducted in triplicate. Data were statistically analyzed using SPSS 20 software and plotted using Origin 9.0 software, and the variability in the data was expressed as the mean  $\pm$  standard deviation.

## Results and discussion

### Characterization of the biochars

The main properties of the six biochars are listed in Tables 1 and 2. The mass yields decreased from 50.41% to 34.90% (spent *Pleurotus ostreatus* substrate biochars) and from 43.45% to 33% (spent shiitake substrate biochars) with an increase in the pyrolysis temperature from 300 °C to 700 °C. However, the ash content increased from 33.27% to 55.71% (spent *Pleurotus ostreatus* substrate biochars) and from 28.02% to 42.28% (spent shiitake substrate biochars). In addition, the pH values of the

biochars derived from the two different raw materials increased from 9.58 to 12.31 and from 10.22 to 12.07, respectively. Previous studies have suggested that biochars obtained at higher temperatures have higher pH values and that the pH increase could be due to the release of alkali salts from the feedstock during pyrolysis.<sup>26,27</sup> The decrease in the content of acidic functional groups such as  $-\text{COOH}$  at high temperature is another factor. As the temperature increased from 300 °C to 700 °C, the concentration of basic functional groups on the biochar surface increased from 0.81 to 4.3 mmol  $\text{g}^{-1}$  (spent *Pleurotus ostreatus* substrate biochars) and from 0.60 to 3.79 mmol  $\text{g}^{-1}$  (spent shiitake substrate biochars), but the concentration of acidic functional groups decreased from 2.06 to 1.15 mmol  $\text{g}^{-1}$  (spent *Pleurotus ostreatus* substrate biochars) and from 1.80 to 0.85 mmol  $\text{g}^{-1}$  (spent shiitake substrate biochars) (Table 2); these trends were consistent with the increase in the pH of the biochar. In our study, the C content of the spent *Pleurotus ostreatus* substrate biochars (PC) decreased with an increase in the pyrolysis temperature, but for the spent shiitake substrate biochars (SC), the C content did not significantly change. In addition, the H, O and N contents and the H/C, O/C and (O + N)/C ratios also decreased. These results suggest that the volatile components, which form a large fraction of the surface functional group elements (C, H, N, and O), are gradually lost during pyrolysis, which is in agreement with the results of a previous study.<sup>28</sup> The H/C molar ratio is an index used to evaluate the degree of carbonization, and a lower H/C ratio in the biochars indicates a more aromatic nature.<sup>29</sup> The O/C and (O + N)/C molar ratios are associated with the polarity and surface oxygen functional groups of the biochars.<sup>30</sup> In this study, the

Table 1 Physical and chemical properties of the biochars<sup>a</sup>

Biochars	Yield (%)	Ash (%)	Elemental analysis				Atomic ratio			pH
			C (%)	H (%)	N (%)	O (%)	H/C	O/C	(O + N)/C	
PC300	50.41	33.27	59.94	2.91	1.75	2.13	0.048	0.036	0.065	9.58
PC500	39.82	52.35	38.73	1.09	0.44	1.69	0.028	0.044	0.055	10.37
PC700	34.90	55.71	37.94	0.99	0.67	0.99	0.026	0.026	0.044	12.31
SC300	43.45	28.02	46.78	2.84	2.71	19.65	0.061	0.420	0.478	10.22
SC500	37.14	35.67	45.92	1.94	2.11	12.36	0.042	0.269	0.315	10.64
SC700	33.00	42.28	44.85	1.23	1.09	9.55	0.028	0.213	0.237	12.07

<sup>a</sup> Spent *Pleurotus ostreatus* substrate biochar (PC), spent shiitake substrate biochar (SC).

Table 2 Microstructure properties and surface functional groups of the biochars<sup>a</sup>

Biochars	BET surface area ( $\text{m}^2 \text{g}^{-1}$ )	Total pore volume ( $\text{mL g}^{-1}$ )	Average pore diameter (nm)	Surface functional groups ( $\mu\text{mol g}^{-1}$ )		
				Acidic	Basic	Carboxylic
PC300	3.79	0.014	14.66	2060.74	803.89	374.16
PC500	18.05	0.061	13.60	1813.15	4880.48	837.49
PC700	188.57	0.134	2.84	1148.62	4300.97	147.55
SC300	12.97	0.028	8.77	1870.43	600.24	539.89
SC500	47.07	0.070	5.97	1359.73	2749.31	189.43
SC700	218.70	0.138	2.52	851.65	3790.90	158.76

<sup>a</sup> Spent *Pleurotus ostreatus* substrate biochar (PC), spent shiitake substrate biochar (SC).



molar ratios of H/C, O/C and (O + N)/C decreased with increasing pyrolysis temperature. These results imply that the biochars acquired at higher pyrolysis temperatures became more aromatic and carbonaceous, and the reduction in the molar ratios of O/C and (O + N)/C indicated a lower polarity and content of oxygen-based functional groups.

The pore structure of the biochars greatly influences the physical adsorption process, and the diffusion rates for Cd(II) transport from the biochar surface to the internal pores are inconsistent because of the presence of different pore structures.<sup>31</sup> Table 2 lists the surface area, total pore volume, average pore diameter and surface functional group contents of the biochars. The data show that the BET surface area increased from 3.79 to 188.57 m<sup>2</sup> g<sup>-1</sup> (spent *Pleurotus ostreatus* substrate biochars) and from 12.97 to 218.70 m<sup>2</sup> g<sup>-1</sup> (spent shiitake substrate biochars) as the pyrolysis temperature increased from 300 °C to 700 °C. The BET surface area of the biochars derived from the spent shiitake substrate was greater than that of the spent *Pleurotus ostreatus* substrate biochars. The BET surface areas of PC700 and SC700 were higher than that of the biochar modified by KMnO<sub>4</sub> impregnation.<sup>32</sup> A higher specific surface area is beneficial for the adsorption of heavy metals by biochar. However, the average pore diameter of the biochars showed a different trend with increasing pyrolysis temperature, which indicated that micropore structures formed more easily in the biochars obtained at higher temperatures.<sup>18</sup> SEM images of the biochars are shown in Fig. 1. When the pyrolysis temperature was 300 °C, the surfaces of PC300 and SC300 contained pores with large diameters because of the rapid volatilization of organic components in the raw materials. Biochars PC500 and SC500 appeared to be layered stacks, and as a result, the surface area was amplified. As the pyrolysis temperature further increased, the surface area increased, and the average number of pores in the biochars (PC700, SC700) decreased because of the formation of a thin and smooth lamellar structure.

The functional groups on the surface of a biochar greatly influence the chemical adsorption process. The cation exchange capacities of biochars are stronger when more oxygen-containing functional groups are present on the surface of the

biochars; hence, the sorption capacities for Cd(II) are also stronger.<sup>31</sup> FT-IR spectroscopy was used to obtain information on the functional groups on the biochar surface, and the results are shown in Fig. S1 and Table S1.† The biochars had various surface oxygen groups and other functional groups (Table S1†). The broad bands from 3200 cm<sup>-1</sup> to 3700 cm<sup>-1</sup> were attributed to -OH stretching vibrations (phenolic, aliphatic or methanol), which can be found in all biochars. The adsorption bands from 1500 cm<sup>-1</sup> to 1650 cm<sup>-1</sup> indicated the presence of aromatic ring C=C and C=O stretching,<sup>32</sup> but these adsorption bands did not appear in SC500 and SC700. A peak was observed at 1426.92 cm<sup>-1</sup> in the spectrum of PC700, which may be associated with the aliphatic CH bending vibration. The absorption observed at 1223.98 cm<sup>-1</sup> in the spectrum of PC300 was attributed to the C-O stretching vibrations of the aryl-alkyl ether linkage and phenol.<sup>33</sup> The absorption peaks in the regions 1360–1430 cm<sup>-1</sup>, 1000–1200 cm<sup>-1</sup>, 700–900 cm<sup>-1</sup> and 400–700 cm<sup>-1</sup> and the corresponding functional groups are listed in Table S1†.<sup>32</sup> For the PC samples, Fig. S1† shows that the adsorption intensities in the 3200–3700 cm<sup>-1</sup> region decreased as the pyrolysis temperature increased, indicating that the number of -OH groups decreased. In addition, the intensity of the adsorption at 1616 cm<sup>-1</sup> decreased, which indicated a reduction in the aromatic ring C=C and C=O stretching; this change was also observed in the SC samples. In all the biochars, the adsorption peak at 1223 cm<sup>-1</sup> disappeared and the peak at 1416 cm<sup>-1</sup> appeared when the temperature increased to 500 °C, which indicated that the functional group content changed with increasing pyrolysis temperature.

### Adsorption of Cd(II) on the biochars

**Adsorption kinetics.** The influence of the reaction time (0–24 h) on Cd(II) adsorption by the different biochars is shown in Fig. 2. Two diverse processes occurred: a rapid initial process in the first few hours and a slow adsorption process to reach the Cd(II) adsorption equilibrium, which occurred at 240, 720, and 240 min for PC300, PC500, and PC700, respectively. Similarly, the adsorption of Cd(II) on SC300, SC500, and SC700 reached equilibrium at 720, 720, and 240 min, respectively. In the

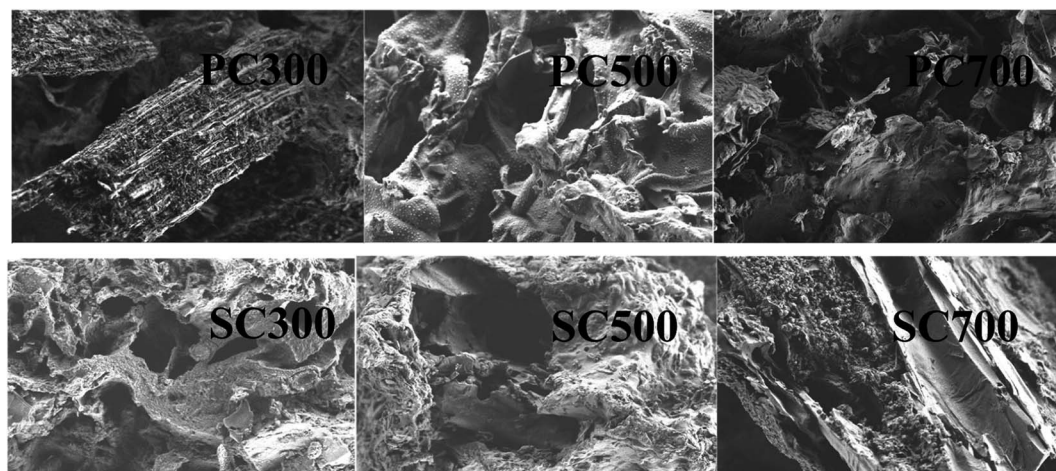


Fig. 1 SEM images of the biochars. Note: spent *Pleurotus ostreatus* substrate biochar (PC) and spent shiitake substrate biochar (SC).





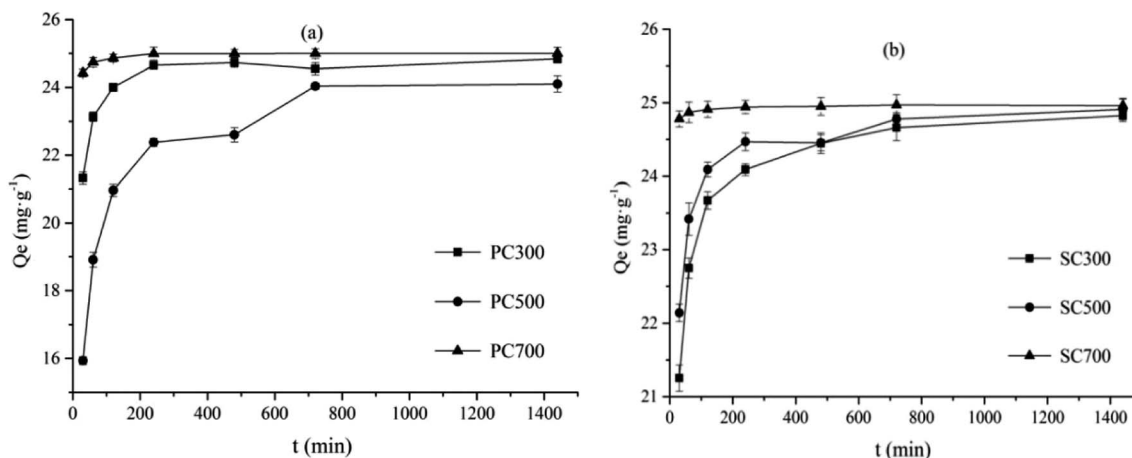


Fig. 2 Adsorption kinetics of Cd(II) onto the different spent *Pleurotus ostreatus* substrate biochar (a) and spent shiitake substrate biochar (b). Note: spent *Pleurotus ostreatus* substrate biochar (PC), spent shiitake substrate biochar (SC).

beginning, adsorption primarily occurred on the outer surfaces of the biochars, and the adsorption mechanism was assumed to be related to physical and chemical adsorption. However, the next stage was relatively slow, which is likely because Cd(II) gradually moved into the pores of the biochars and further reacted with the internal active sites, and the adsorption capacity ultimately reached saturation over time.

The pseudo-first-order and pseudo-second-order kinetics models were used to evaluate the adsorption kinetics and mechanism of solid-liquid adsorption:<sup>34</sup>

$$\ln(Q_e - Q_t) = \ln Q_e - k_1 t \quad (3)$$

$$t/Q_t = 1/k_2 Q_e^2 + t/Q_e \quad (4)$$

where  $Q_t$  and  $Q_e$  represent the adsorption capacity at time  $t$  (min) and at equilibrium (mg g<sup>-1</sup>), respectively, and  $k_1$  (min<sup>-1</sup>) and  $k_2$  (g mg<sup>-1</sup> min<sup>-1</sup>) are the adsorption rate constants for the pseudo-first-order and pseudo-second-order adsorption processes, respectively.

The Cd(II) adsorption data for the different biochars were fitted using the above two adsorption kinetics models. As shown by the data in Table 3, Cd(II) adsorption by the biochars was better fitted by the pseudo-second-order model (correlation coefficients ( $R^2$ ) > 0.9895) (Table 3). In addition, the adsorption

capacity ( $Q_e$ ) values acquired from the pseudo-second-order model fitting were more consistent with the experimental values ( $Q_{exp}$ ). Therefore, the pseudo-second-order kinetics model better described the mechanism of Cd(II) adsorption by the biochars. This result, which indicated that adsorption occurred primarily through chemisorption, is in agreement those of with previous studies.<sup>33</sup>

**Adsorption isotherm.** The adsorption isotherms for Cd(II) on different biochars are shown in Fig. 3. In our study, four well-known models, the Langmuir, Freundlich, Temkin and Dubinin-Radushkevich (D-R) isotherm models, were selected to fit the Cd(II) adsorption data, and the fitting constants of the four models are listed in Table 4.

The Langmuir adsorption isotherm equation can be expressed as<sup>35</sup>

$$Q_e = Q_m K_L C_e / (1 + K_L C_e) \quad (5)$$

where  $C_e$  represents the equilibrium aqueous concentration of Cd(II) (mg L<sup>-1</sup>),  $Q_e$  represents the adsorption capacity at equilibrium (mg g<sup>-1</sup>), and  $K_L$  (L mg<sup>-1</sup>) and  $Q_m$  (mg g<sup>-1</sup>) represent the Langmuir constant and the maximum adsorption capacity, respectively.

Table 3 Fitting parameters of the pseudo-first-order and pseudo-second-order kinetics models that describe Cd(II) adsorption on different biochars<sup>a</sup>

Biochars	$Q_{exp}$ (mg g <sup>-1</sup> )	Pseudo-first-order			Pseudo-second order		
		$Q_e$ (mg g <sup>-1</sup> )	$k_1$ (min <sup>-1</sup> )	$R^2$	$Q_e$ (mg g <sup>-1</sup> )	$k_2$ (g mg <sup>-1</sup> min <sup>-1</sup> )	$R^2$
PC300	24.84	24.43	0.0663	0.8466	25	0.0079	0.9903
PC500	24.10	22.83	0.0352	0.8156	23.92	0.0027	0.9895
PC700	25.00	24.94	0.1293	0.7641	25.06	0.0542	0.9914
SC300	24.83	24.19	0.0673	0.7464	24.75	0.0081	0.9935
SC500	24.91	24.42	0.0769	0.7710	24.81	0.0110	0.9911
SC700	24.96	24.94	0.1694	0.6893	24.94	0.1748	0.9913

<sup>a</sup> Spent *Pleurotus ostreatus* substrate biochar (PC) and spent shiitake substrate biochar (SC).



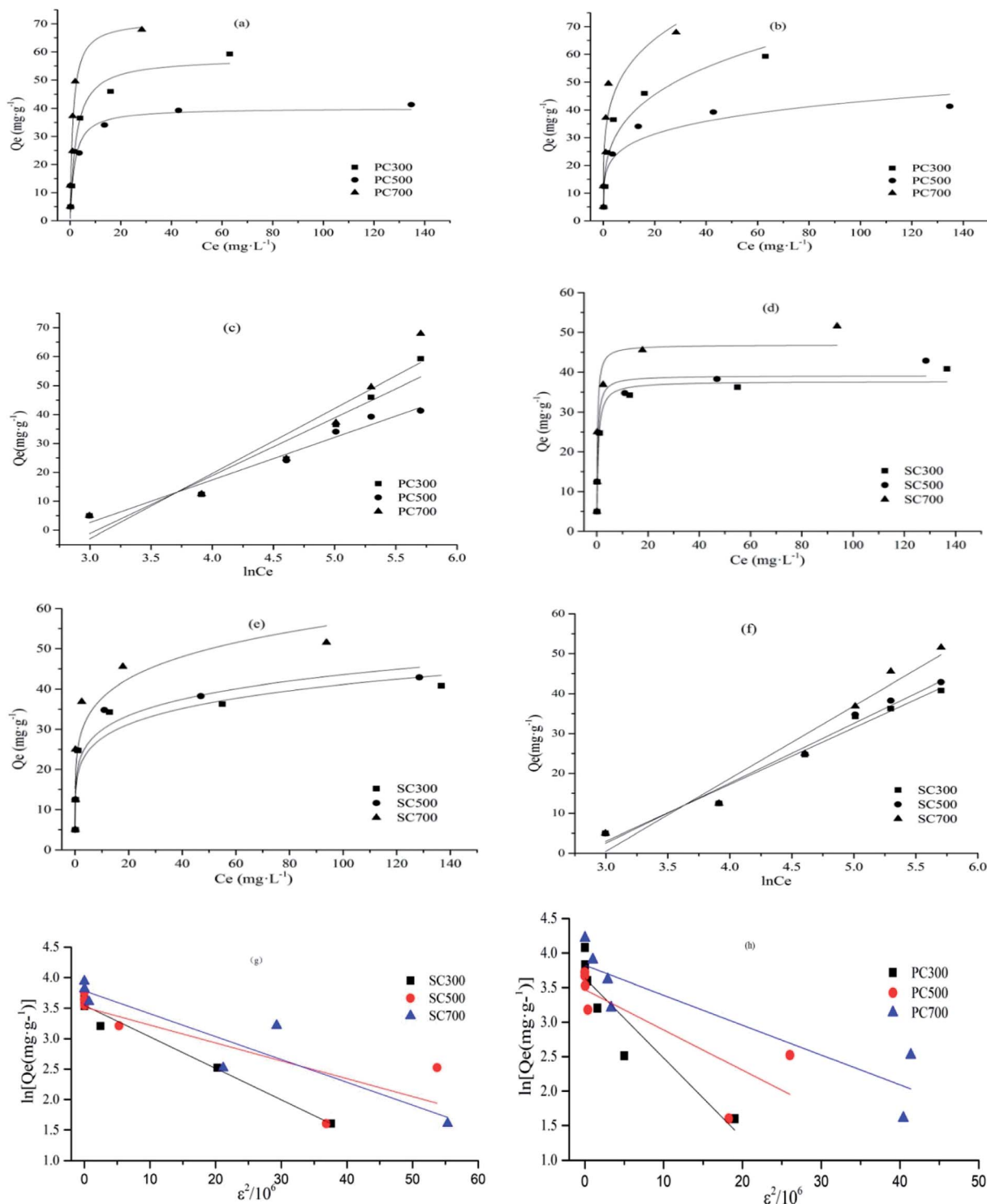


Fig. 3 Adsorption isotherms of Cd(II) onto different biochars, Langmuir adsorption isotherms for Cd(II) adsorption onto the different spent *Pleurotus ostreatus* substrate biochar (a) and spent shiitake substrate biochar (d). Freundlich adsorption isotherms for Cd(II) adsorption onto the different spent *Pleurotus ostreatus* substrate biochar (b) and spent shiitake substrate biochar (e). Temkin adsorption isotherms for Cd(II) adsorption onto the different spent *Pleurotus ostreatus* substrate biochar (c) and spent shiitake substrate biochar (f). D-R model for Cd(II) adsorption onto the different spent shiitake substrate biochar (g) and spent *Pleurotus ostreatus* substrate biochar (h). Note: spent *Pleurotus ostreatus* substrate biochar (PC), spent shiitake substrate biochar (SC).



Table 4 Adsorption isotherm constants for the Cd(II) by biochars<sup>a</sup>

Biochars	Langmuir model			Freundlich model			Temkin model			D-R model			
	$Q_m$ (mg g <sup>-1</sup> )	$K_L$ (L mg <sup>-1</sup> )	$R^2$	$K_F$ (mg <sup>(1-n)</sup> L <sup>n</sup> g <sup>-1</sup> )	$n$	$R^2$	$A$	$B$	$R^2$	$Q_m$ (mg g <sup>-1</sup> )	$\beta$ (mol <sup>2</sup> K <sup>-1</sup> J <sup>-2</sup> )	$E$ (kJ mol <sup>-1</sup> )	$R^2$
PC300	57.95	0.429	0.9784	19.76	3.59	0.8956	0.047	20.02	0.9123	38.03	0.116	2.08	0.8204
PC500	40.14	0.567	0.8849	17.34	5.07	0.8664	0.059	14.75	0.9594	32.22	0.058	2.93	0.5842
PC700	71.49	0.889	0.8944	33.22	4.42	0.8882	0.044	22.51	0.8708	45.73	0.043	3.40	0.7716
SC300	37.67	1.945	0.9727	18.75	5.87	0.8461	0.062	14.21	0.9685	34.78	0.052	3.10	0.9724
SC500	40.99	2.683	0.9687	21.27	6.08	0.7897	0.716	15.01	0.9678	33.74	0.029	3.25	0.5959
SC700	46.87	3.534	0.8519	25.27	5.75	0.7940	0.059	18.21	0.9425	44.08	0.038	3.63	0.8269

<sup>a</sup> Spent *Pleurotus ostreatus* substrate biochar (PC) and spent shiitake substrate biochar (SC).

The Freundlich adsorption isotherm equation can be represented as<sup>35</sup>

$$Q_e = K_F C_e^{1/n} \quad (6)$$

where  $K_F$  (mg<sup>(1-n)</sup> L<sup>n</sup> g<sup>-1</sup>) and  $1/n$  are Freundlich constants that represent the adsorption density and intensity, respectively.

The Temkin isotherm model can be represented in linear form as<sup>35</sup>

$$Q_e = B \ln A + B \ln C_e \quad (7)$$

where  $A$  and  $B$  are the Temkin constants.

The Dubinin–Radushkevich (D–R) isotherm model is given as<sup>35</sup>

$$\ln Q_e = \ln Q_m - \beta \varepsilon^2 \quad (8)$$

where  $\varepsilon = RT \ln \left(1 + \frac{1}{C_e}\right)$ ,  $R$  is the gas constant (8.314 J mol<sup>-1</sup> K<sup>-1</sup>) and  $T$  is the temperature (298 K).  $\beta$  is the Dubinin–Radushkevich isotherm constant (mol<sup>2</sup> K<sup>-1</sup> J<sup>-2</sup>).

The approach was applied to distinguish the physical and chemical adsorption of metal ions according to the mean free energy,  $E$ , per molecule of adsorbate, which can be calculated by<sup>35</sup>

$$E = \frac{1}{\sqrt{2\beta}} \quad (9)$$

Based on the fitting constants and correlation coefficients ( $R^2$ ) of the four models for all the biochars, the Langmuir and Temkin models fit the Cd(II) adsorption experimental data well. The results demonstrate that Cd(II) adsorption primarily occurred on monolayers or through a fixed number of identical, energetically equivalent sites on the surface.<sup>32</sup> The dimensionless separation factor ( $R_L = 1/(1 + bC_o)$ ) is the essential characteristic index of the Langmuir isotherm model.  $C_o$  (mg g<sup>-1</sup>) represents the initial Cd concentration, and  $b$  (L mg<sup>-1</sup>) is the Langmuir constant. Adsorption is unfavorable when  $R_L > 1$ ; when  $R_L = 1$ , adsorption is linear; when  $0 < R_L < 1$ , adsorption is favorable; and when  $R_L = 0$ , adsorption is irreversible.<sup>36</sup> In this study, the  $R_L$  values ranged

between 0.001 and 0.104, revealing that Cd(II) adsorption by the biochars is a favorable process.

Studies have shown that a favorable adsorption process tends to have a Freundlich constant,  $n$ , between 1 and 10, and the interactions between the biochar and heavy metal ions are stronger when the  $n$  value is higher.<sup>37</sup> In this study, the  $n$  values ranged between 3.59 and 6.08. Among the PC and SC biochars, PC500 and SC500 had the maximum  $n$  values. These results show that the biochars obtained at 300 °C and 700 °C were more heterogeneous than the biochars obtained at 500 °C. Furthermore, the Temkin isotherm better fit the Cd(II) adsorption data than the other models, which indicated that the adsorption process was primarily controlled by chemical adsorption through electrostatic interactions.<sup>18,38</sup> This result is consistent with the fact that the adsorption equilibrium data were well represented by the pseudo-second-order adsorption model. The constant  $E$  derived from the fitting constants of the D–R model suggests the type of adsorption mechanism that is operative. Generally, physical interactions exist during the adsorption process when the value of  $E$  is in the range of 1–8 kJ mol<sup>-1</sup>, while a value of  $E$  in the range 8–16 kJ mol<sup>-1</sup> suggests the occurrence of ion exchange, and an  $E$  value in the range 16–40 kJ mol<sup>-1</sup> indicates that chemical adsorption is operative.<sup>39</sup> In this study, the value of  $E$  was in the range 2.08–3.63, indicating that physical interactions existed simultaneously in the adsorption process. For PC and SC, the maximum value of  $E$  occurred for the biochars obtained at higher temperatures. This trend mainly occurred because PC700 and SC700 possessed larger BET surface areas than the other biochars, which is beneficial for physical adsorption.

As shown in Table 3, the maximum adsorption capacities ( $Q_m$ ) of PC700 and SC700 were 71.49 and 46.87 mg g<sup>-1</sup>, respectively. Thus, higher  $Q_m$  values were obtained for the high-temperature biochars, and the above values differed because different raw materials were employed, which introduced varying physical and/or chemical characteristics in the biochars. The  $Q_m$  values obtained in our study are equivalent to or even higher than those obtained for other biochars (Table S2†). Therefore, these results clearly indicate that the biochars prepared in our study are effective adsorbents for Cd(II) removal from wastewater.



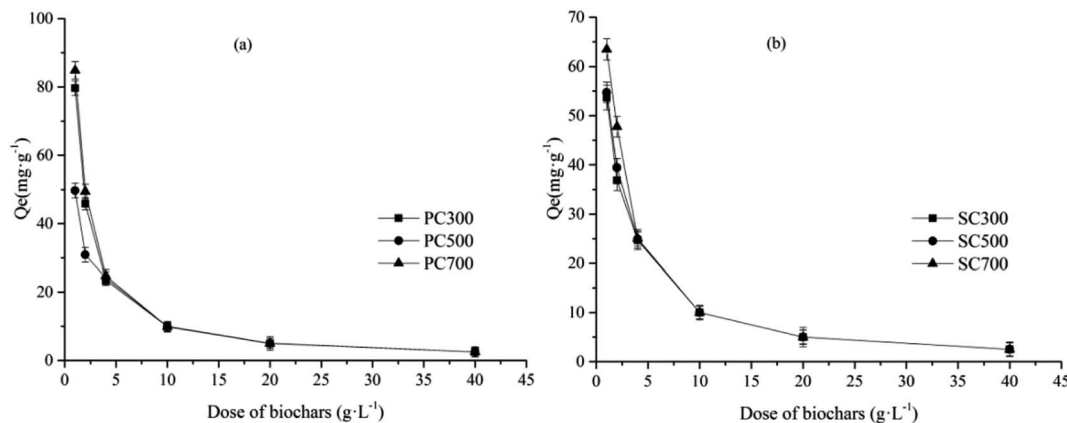


Fig. 4 Effects of biochar mass on the adsorption of Cd(II) by different spent *Pleurotus ostreatus* substrate biochars (a) and spent shiitake substrate biochars (b). Note: spent *Pleurotus ostreatus* substrate biochar (PC), spent shiitake substrate biochar (SC).

### Effect of the adsorbent mass

The influence of the amount of biochar on the Cd(II) adsorption capacity is summarized in Fig. 4. Some differences in the Cd(II) adsorption capacity were observed between the biochars prepared at different temperatures and from different raw materials. The Cd(II) adsorption capacities of the high-temperature biochars (PC700 and SC700) were higher than those of the other biochars. Among the biochars from different raw materials, the Cd(II) adsorption capacities of the PC biochars were higher than those of the SC biochars because the type of biochar feedstock affects the physical and chemical properties of the biochar. The Cd(II) adsorption capacity decreased and the Cd(II) removal efficiency increased with an increase in the amount of biochar. Previous studies on the

adsorption of heavy metals suggested that the number of negatively charged sites available for metal adsorption and the amount of biochar used for batch experiments have a direct, proportional relationship.<sup>33</sup> Therefore, the Cd(II) removal efficiency increased with an increase in the number of sites. However, the adsorption capacity decreased as the amount of biochar increased because of the presence of more adsorption sites, but the capacity did not reach saturation when the Cd ion concentration in solution was at a certain level.

### Effect of the pH

Studies have suggested that the initial pH of the solution employed in adsorption experiments is a significant parameter that affects the adsorption of heavy metals by influencing the

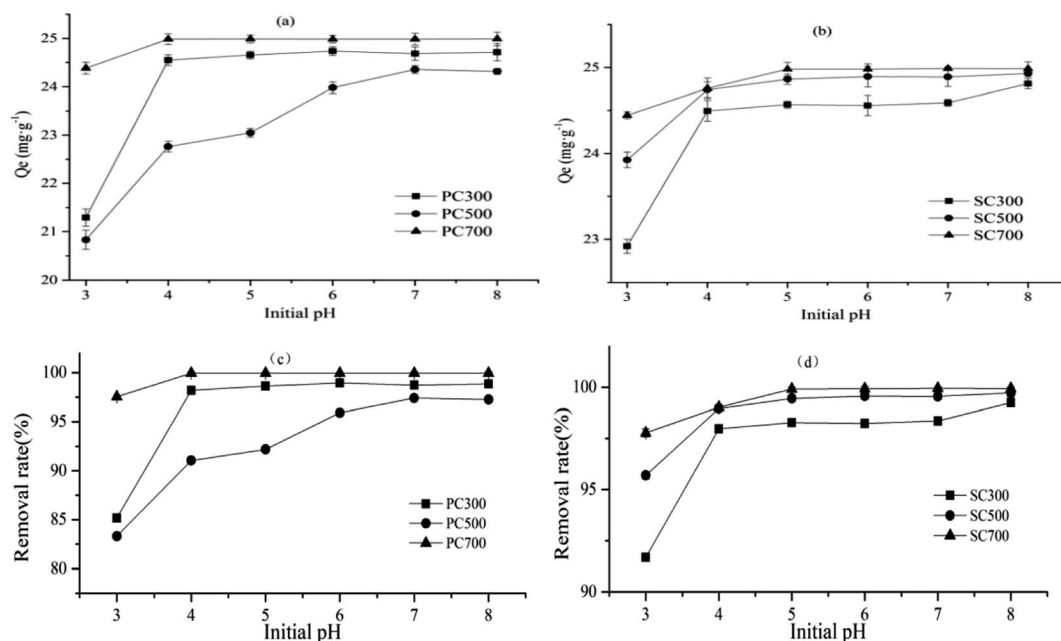


Fig. 5 Effects of initial pH on Cd(II) adsorption capacity by different spent *Pleurotus ostreatus* substrate biochars (a) and spent shiitake substrate biochars (b). And the effect of pH on removal rate of Cd(II) by different spent *Pleurotus ostreatus* substrate biochars (c) and spent shiitake substrate biochars (d). Note: spent *Pleurotus ostreatus* substrate biochar (PC), spent shiitake substrate biochar (SC).





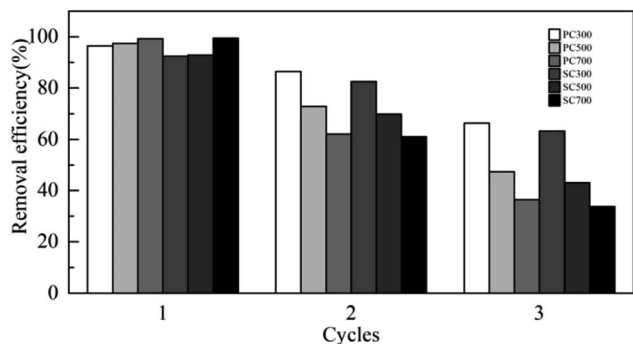


Fig. 6 The removal efficiency of Cd(II) in solution using spent mushroom substrate biochars over three consecutive adsorption-desorption cycles. Note: spent *Pleurotus ostreatus* substrate biochar (PC), spent shiitake substrate biochar (SC).

charge of the absorbent surface, ionization of the surface functional groups and speciation of the adsorbate.<sup>40,41</sup> The influence of the initial pH on Cd(II) adsorption by the biochars is summarized in Fig. 5. As shown in Fig. 5, the removal ratio of Cd(II) gradually increased with the initial pH. In addition, the removal ratio of Cd(II) was above 95% when the initial pH was in the range of 4–7 for all biochars. The difference in removal efficiency under acidic conditions is largely related to the change in the surface charge of the adsorbent during the adsorption process. Initially, the adsorption capacity rapidly increased when the initial solution pH increased from 3 to 4 for PC500, PC700, SC300, SC500 and SC700, and for PC500, the adsorption capacity rapidly increased when the initial solution pH increased from 3 to 7. Subsequently, the adsorption capacity was stable between pH 4 and 7 for all biochars except PC500. This study suggests that more protons competed with the metal cations for the adsorption sites because hydronium ions were closely associated with the absorbent surface at low pH values.<sup>42</sup> As the pH value increased, the hydronium ion concentration decreased, and the functional groups on the absorbent surface became negatively charged, making the absorbent surface more available for metal ion adsorption.<sup>40</sup> Therefore, the adsorption

capacity increased. Several studies have also shown a similar pH effect on the adsorption of heavy metals using different types of biochars.<sup>32,33</sup>

### Reusability studies of spent mushroom substrate biochars

To test the reusability of the SMS biochars, three consecutive adsorption cycles were performed in triplicate. The removal efficiency of Cd(II) in solution using the SMS biochars decreased gradually over three consecutive adsorption-desorption cycles, as shown in Fig. 6. In the first cycle, the removal ratio of Cd(II) by all biochars was over 90%. For PC300 and SC300, the removal ratio of Cd(II) in the second cycle was 86% and 83%, respectively, and in the third cycle, the removal efficiency of Cd(II) dropped to 66% and 63%, respectively. However, for the other biochars, in the third cycle, the removal efficiency of Cd(II) was less than 50%. Thus, the results show that the reusability of the biochars acquired at higher temperatures for Cd(II) adsorption was not as good as that of the biochars obtained at lower temperatures. This difference might be because the adsorption sites of the biochars obtained at higher temperatures were rapidly occupied by Cd(II) ions in solution in the first cycle.

### Possible mechanisms of Cd(II) adsorption by the biochars

According to the Cd(II) adsorption kinetics and isotherms of the biochars, the adsorption process was primarily controlled by chemical adsorption through electrostatic interactions. The chemical interactions between cadmium and the surface of the biochars were clarified by analyzing the FT-IR spectra of the biochars and biochar-Cd complexes. As shown in Fig. 7, the adsorption bands of biochar-Cd at 3200–3700 cm<sup>-1</sup>, 2330–2370 cm<sup>-1</sup>, 1500–1650 cm<sup>-1</sup>, 1360–1430 cm<sup>-1</sup> and 400–700 cm<sup>-1</sup> changed compared with those of the Cd-free biochar, which indicated that –OH, –NH<sub>2</sub>, carbonyl, and other functional groups participated in the chemical adsorption process. To identify the possible formation of crystalline Cd minerals, PC and SC were comparatively analyzed before and after Cd sorption by XRD. As shown in Fig. 8, the peaks of biochar-Cd at 27–28 degrees indicated the precipitation of CdCO<sub>3</sub> on the surface

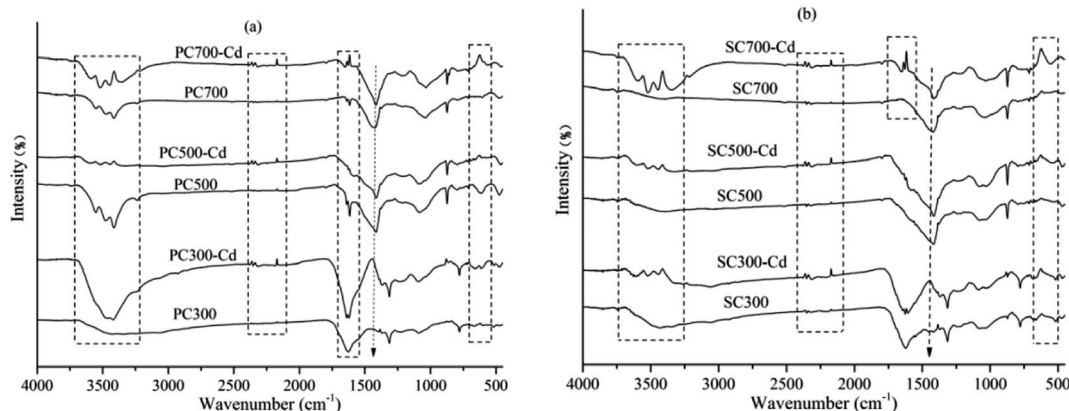


Fig. 7 The FT-IR spectra of the biochars before (PC300, PC500 and PC700) and after (PC300-Cd, PC700-Cd and PC700-Cd) the adsorption of Cd (a) and the biochars before (SC300, SC500 and SC700) and after (SC300-Cd, SC700-Cd and SC700-Cd) the adsorption of Cd (b). Note: spent *Pleurotus ostreatus* substrate biochar (PC), spent shiitake substrate biochar (SC).



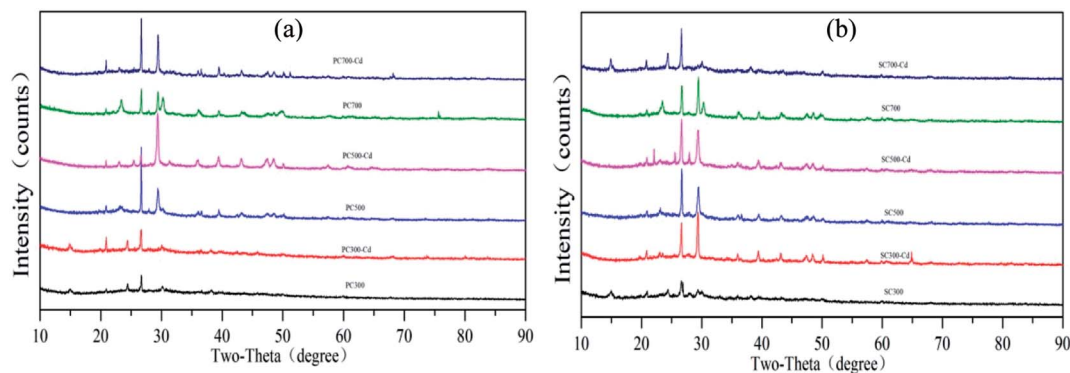


Fig. 8 The XRD patterns of the biochars before (PC300, PC500 and PC700) and after (PC300-Cd, PC700-Cd and PC700-Cd) the adsorption of Cd (a) and the biochars before (SC300, SC500 and SC700) and after (SC300-Cd, SC700-Cd and SC700-Cd) the adsorption of Cd (b). Note: spent *Pleurotus ostreatus* substrate biochar (PC), spent shiitake substrate biochar (SC).

of the biochars. In addition, the peaks of biochar-Cd at 29–30 degrees indicated the precipitation of a smaller amount of  $\text{Cd}_3(\text{PO}_4)_2$  on the surface of the biochars. Based on other reported works,<sup>43,44</sup> the possible mechanisms for Cd(II) adsorption by the biochars are as follows: (1) Cd complexation with the oxygenated functional groups, (2)  $\text{Cd}^{2+}$ - $\pi$  interaction formation, and (3) surface precipitation of Cd carbonates.

## Conclusions

The physical and chemical properties of biochars are significantly affected by an increase in the pyrolysis temperature, which is beneficial for Cd(II) adsorption. The Langmuir and Temkin isotherm models describe Cd(II) adsorption better than the Freundlich model does, and the adsorption kinetics are well described by the pseudo-second-order model. Among the biochars derived from different raw materials, the maximum adsorption capacities of PC700 and SC700 are 71.49 and 46.87 mg  $\text{g}^{-1}$ , respectively, which show that the biochars in our study can be effective adsorbents for Cd(II) removal from wastewater. The data in the present study indicate that the amount of biochar and the initial solution pH also affect Cd(II) adsorption, and a good adsorption capacity is obtained for a biochar dose of 4.0 g  $\text{L}^{-1}$ , pH between 4 and 7, and adsorption time of 12 h. The FT-IR spectra and XRD patterns of the biochars before and after Cd(II) adsorption indicate that the possible mechanisms of adsorption are Cd complexation with the oxygenated functional groups,  $\text{Cd}^{2+}$ - $\pi$  interaction formation and surface precipitation of Cd carbonates. However, the specific adsorption mechanism must be further investigated in detail.

## Conflicts of interest

There are no conflicts to declare.

## Acknowledgements

This work was supported by the Provincial Science and Technology Support Program of Sichuan (Grant No. 2016NZ0039 and 2015SZ0007).

## References

- 1 F. J. Gea, M. Santos, F. Dianez, J. C. Tello and M. J. Navarro, *World J. Microbiol. Biotechnol.*, 2012, **28**, 2765–2769.
- 2 Z. Lou, Y. Sun, S. Bian, S. Ali Baig, B. Hu and X. Xu, *Chemosphere*, 2017, **169**, 23–31.
- 3 C. Paredes, E. Medina, R. Moral, M. D. Pérez-Murcia, J. Moreno-Caselles, M. Angeles Bustamante and J. A. Cecilia, *Commun. Soil Sci. Plant Anal.*, 2009, **40**, 150–161.
- 4 A. A. Bakar, N. Z. Mahmood, J. A. Teixeira da Silva, N. Abdullah and A. A. Jamaludin, *Biotechnol. Bioprocess Eng.*, 2011, **16**, 1036.
- 5 G.-j. Chen, C.-y. Peng, J.-y. Fang, Y.-y. Dong, X.-h. Zhu and H.-m. Cai, *Desalin. Water Treat.*, 2015, **57**, 12385–12395.
- 6 N. Liu, C. J. Zhou, S. F. Fu, M. I. Ashraf, E. F. Zhao, H. Shi, X. R. Han and Z. B. Hong, *Adv. Mater. Res.*, 2013, **724–725**, 452–456.
- 7 N. H. Ab Razak, S. M. Praveena, A. Z. Aris and Z. Hashim, *J. Epidemiol. Glob. Health*, 2015, **5**, 297–310.
- 8 B. Wei and L. Yang, *Microchem. J.*, 2010, **94**, 99–107.
- 9 Y. Jiang, S. Chao, J. Liu, Y. Yang, Y. Chen, A. Zhang and H. Cao, *Chemosphere*, 2017, **168**, 1658–1668.
- 10 S. Khan, S. Rehman, A. Z. Khan, M. A. Khan and M. T. Shah, *Ecotoxicol. Environ. Saf.*, 2010, **73**, 1820–1827.
- 11 Y. Liu, T. Xiao, Z. Ning, H. Li, J. Tang and G. Zhou, *Appl. Geochem.*, 2013, **37**, 149–156.
- 12 X. Wang, *Int. J. Geosci.*, 2013, **04**, 309–316.
- 13 H. Y. Yu, C. Liu, J. Zhu, F. Li, D. M. Deng, Q. Wang and C. Liu, *Environ. Pollut.*, 2016, **209**, 38–45.
- 14 D. A. Laird, R. C. Brown, J. E. Amonette and J. Lehmann, *Biofuels, Bioprod. Biorefin.*, 2009, **3**, 547–562.
- 15 M. I. Silva, C. Mackowiak, P. Minogue, A. F. Reis and E. F. d. V. Moline, *Cienc. Rural*, 2017, **47**, 1–5.
- 16 R. Conti, D. Fabbri, I. Vassura and L. Ferroni, *J. Anal. Appl. Pyrolysis*, 2016, **122**, 160–168.
- 17 B. Liang, J. Lehmann, D. Solomon, J. Kinyangi, J. Grossman, B. O'Neill, J. O. Skjemstad, J. Thies, F. J. Luizão, J. Petersen and E. G. Neves, *Soil Sci. Soc. Am. J.*, 2006, **70**, 1719–1730.



- 18 G. Yang, L. Wu, Q. Xian, F. Shen, J. Wu and Y. Zhang, *PLoS One*, 2016, **11**, e0154562.
- 19 R. Davarnejad and P. Panahi, *J. Ind. Eng. Chem.*, 2016, **33**, 270–275.
- 20 M. E. Doumer, A. Rigol, M. Vidal and A. S. Mangrich, *Environ. Sci. Pollut. Res. Int.*, 2016, **23**, 2684–2692.
- 21 H. Wang, B. Gao, S. Wang, J. Fang, Y. Xue and K. Yang, *Bioresour. Technol.*, 2015, **197**, 356–362.
- 22 W.-Q. Zuo, C. Chen, H.-J. Cui and M.-L. Fu, *RSC Adv.*, 2017, **7**, 16238–16243.
- 23 Y.-Y. Wang, H.-Y. Ji, H.-H. Lu, Y.-X. Liu, R.-Q. Yang, L.-L. He and S.-M. Yang, *RSC Adv.*, 2018, **8**, 3264–3273.
- 24 H. P. Boehm, *Carbon*, 1994, **32**, 759–769.
- 25 J. R. Rangel-Mendez and M. Streat, *Water Res.*, 2002, **36**, 1244–1252.
- 26 R. Goswami, J. Shim, S. Deka, D. Kumari, R. Kataki and M. Kumar, *Ecol. Eng.*, 2016, **97**, 444–451.
- 27 Y. Shinogi and Y. Kanri, *Bioresour. Technol.*, 2003, **90**, 241.
- 28 T. Chen, Y. Zhang, H. Wang, W. Lu, Z. Zhou, Y. Zhang and L. Ren, *Bioresour. Technol.*, 2014, **164**, 47–54.
- 29 A. Hmid, D. Mondelli, S. Fiore, F. P. Fanizzi, Z. Al Chami and S. Dumontet, *Biomass Bioenergy*, 2014, **71**, 330–339.
- 30 M. I. Al-Wabel, A. Al-Omran, A. H. El-Naggar, M. Nadeem and A. R. Usman, *Bioresour. Technol.*, 2013, **131**, 374–379.
- 31 M. Ahmad, A. U. Rajapaksha, J. E. Lim, M. Zhang, N. Bolan, D. Mohan, M. Vithanage, S. S. Lee and Y. S. Ok, *Chemosphere*, 2014, **99**, 19–33.
- 32 B. Li, L. Yang, C. Q. Wang, Q. P. Zhang, Q. C. Liu, Y. D. Li and R. Xiao, *Chemosphere*, 2017, **175**, 332–340.
- 33 Q. Cheng, Q. Huang, S. Khan, Y. Liu, Z. Liao, G. Li and Y. S. Ok, *Ecol. Eng.*, 2016, **87**, 240–245.
- 34 H. Liu, X. Cai, Y. Wang and J. Chen, *Water Res.*, 2011, **45**, 3499–3511.
- 35 X.-b. Li, J.-j. Ye, Z.-h. Liu, Y.-q. Qiu, L.-j. Li, S. Mao, X.-c. Wang and Q. Zhang, *J. Cent. South Univ.*, 2018, **25**, 9–20.
- 36 M. Gorgievski, D. Božić, V. Stanković, N. Štrbac and S. Šerbula, *Ecol. Eng.*, 2013, **58**, 113–122.
- 37 A. S. Krishna Kumar, T. Gupta, S. S. Kakan, S. Kalidhasan, Manasi, V. Rajesh and N. Rajesh, *J. Hazard. Mater.*, 2012, **239–240**, 213–224.
- 38 Y. Gao, Y. Li, L. Zhang, H. Huang, J. Hu, S. M. Shah and X. Su, *J. Colloid Interface Sci.*, 2012, **368**, 540–546.
- 39 S. Fan, H. Li, Y. Wang, Z. Wang, J. Tang, J. Tang and X. Li, *Res. Chem. Intermed.*, 2017, **44**, 135–154.
- 40 M. Moyo, U. Guyo, G. Mawenyiyo, N. P. Zinyama and B. C. Nyamunda, *J. Ind. Eng. Chem.*, 2015, **27**, 126–132.
- 41 R. A. Anayurt, A. Sari and M. Tuzen, *Chem. Eng. J.*, 2009, **151**, 255–261.
- 42 M. Mohapatra, L. Mohapatra, P. Singh, S. Anand and B. K. Mishra, *International Journal of Engineering, Science and Technology*, 2010, **2**, 89–103.
- 43 H. Li, X. Dong, E. B. da Silva, L. M. de Oliveira, Y. Chen and L. Q. Ma, *Chemosphere*, 2017, **178**, 466–478.
- 44 F. Zhang, X. Wang, D. Yin, B. Peng, C. Tan, Y. Liu, X. Tan and S. Wu, *J. Environ. Manage.*, 2015, **153**, 68–73.

